Chem. Eng. Comm., 201:102–119, 2014

ISSN: 0098-6445 print/1563-5201 online
DOI: 10.1080/00986445.2012.762628

Taylor & Francis
Taylor & Francis Group

Analytical Model of Local Distribution of Chemicals in Tissues with First-Order-Rate Metabolism Kinetics

ALEXANDER GOLBERG

Department of Mechanical Engineering, University of California at Berkeley, Berkeley, California, USA

The profile of regional distribution of chemicals in tissue is important for the development of novel locally applied therapies. Here we introduce an analytical approach for the temporal and spatial regional distribution of chemicals in living tissues. The new aspect of this model is in local chemical concentration dependence on the tissue perfusion rate, in addition to diffusion and metabolism rates. Using the Duhamel theorem we performed dimensionless and dimensional analysis for local chemical distribution and report on steady-state and transient solutions for tissues with the first-order kinetic rate of clearance by perfusion and metabolism. The predictions of our model are in good correlation with clinically observed data on percutaneous ethanol ablation of liver. Our results emphasize the importance of mathematical modeling that includes perfusion in the planning of therapies with local chemical distribution in living tissues.

Keywords Electro chemotherapy; Percutaneous ethanol injection; Regional diffusion; Transport phenomena in tissues

Introduction

Once introduced to tissue, chemical species diffuse, decompose, are metabolized by cells, absorb to cell membranes and extracellular matrix, and are washed out by body fluids by a process called "clearance" (Kwon, 2001). Understanding regional transport phenomena in living tissue is important for local therapy development. However, living tissues are extremely complex systems and have multiple processes that affect transport phenomena (Saltzman, 2001).

Various regional therapies use the direct injection of chemical species to tissues. For example, ethanol and acetic acid are injected percutaneously for ablation of hepatocellular carcinoma (Schlag and Stein, 2007; Tsai et al., 2008), parathyroid tumors (Bennedbaek et al., 1997), skin melanoma (Nakayama et al., 1997), pancreatic cystic lesions (DiMaio et al., 2011), benign prostatic hyperplasia (Goya et al., 1999), benign nodular and cystic thyroid diseases (Lee and Ahn, 2005), and bone metastases (Gangi et al., 1994). In addition, local anesthetic maldistribution is

Address correspondence to Alexander Golberg, Center for Engineering in Medicine, Department of Surgery, Massachusetts General Hospital, Harvard Medical School and Shriners Burn Hospital for Children, 51 Blossom Street, Boston, MA 02114, USA. E-mail: agolberg@gmail.com

thought to be one of the causes of cauda equina syndrome (Myers, 1996; Ross et al., 1992); thus, there is interest in the spatial and temporal distribution of a locally injected anesthetic in the body for local anesthesia procedures (Doherty et al., 1995; Ummenhofer et al., 2000).

Furthermore, electrochemotherapy (ECT), an emerging clinical method for tumor treatment, involves direct injection of chemotherapeutical drugs such as bleomycin and cicplatin into tumors (Gothelf et al., 2003; Heller et al., 1999). Following the injection, pulse electric fields are applied to facilitate efficient drug transport from the intracellular space to the cells (Mir et al., 1991; Sersa et al., 2008). Additional emerging personal therapies, such as electro-gene therapy, require that the whole region of interest is covered with an appropriate concentration of specific DNA and RNA molecules before the application of electric fields (Andre and Mir, 2004; Paganin-Gioanni et al., 2011).

One of the challenges for regional therapies is the synchronization among the injected dose, time, toxicity level, and treatment efficiency. Therefore, real-time imaging and optimization experiments are performed today to define and control the treatment protocols. For instance, real-time ultrasound (Heilo et al., 2011; Papini et al., 1993) or MRI (Kim et al., 2005) is used today to control percutaneous ethanol injection therapy (PEIT) to insure full coverage of the area of interest with ethanol. In the currently applied ECT protocol, synchronization between the pharmaceutical injection and the delivery of pulse electric fields is done by trial and error. Specifically, optimization experiments are performed to find the most effective time between the injection of a specific drug and application of a pulse electric field (Cemazar et al., 1998; Glass et al., 1997). In these studies, chemotherapy drugs are injected at various time points before and after the delivery of pulse electric fields, and post-treatment tumor growth is monitored. Even though specific recommendations for the injected volume of drugs have been published, synchronization between the drug injection and pulse delivery varies among reports (Cemazar et al., 1998; Glass et al., 1997; Heller et al., 1999).

A critical role in the distribution profile of the injected chemicals is played by "clearance" or washing out. The clearance rate depends on tissue perfusion levels with body fluids. Starting with Pennes's seminal work in 1948, the critical role of tissue perfusion levels was investigated by bioheat groups in the context of body thermoregulation (Pennes, 1948; Shitzer, 2011). An important conclusion from bioheat studies in the field of cryobiology and thermal tissue ablation is that tissue perfusion level limits externally induced heat propagation in living tissues (Nakayama et al., 2011). Thus, it was analytically and experimentally shown that a cryogenic probe with a certain diameter and temperature could freeze a limited volume of tissue, the radius of which was defined by blood perfusion levels (Nakayama et al., 2011).

Mathematical modeling of biotransport phenomena is an important tool in drug delivery planning, cell signaling, and tissue engineering research (Baish et al., 2011; Eungdamrong and Iyengar, 2004). Upton et al. (1991) reviewed analyses of regional drug clearance due to blood perfusion. The models, however, deal with the transfer and clearance function and do not incorporate metabolism and temporal and spatial distribution of the drug in the tissue. Due to the critical clinical consequences of maldistribution during spinal anesthesia, Myers (1996) developed a numerical model to analyze various factors that affect spinal anesthetic distribution. Saltzman and Radomsky (1991) introduced a numerical model that incorporates cell uptake and

elimination for drugs released by diffusion from polymers in the brain. Shen et al. (2006) studied naked DNA diffusion in mucus, aiming at the development of a tool set for future personalized gene therapy. These models, however, do not describe the spatial-temporal distribution of chemical species in perfused, metabolically active tissues. Furthermore, in clinical therapies such as PEIT and ECT the volumes of locally administrated drugs are based today on the calculated tumor size and depend on assumed, simplified tumor geometry (Mir et al., 2006; Schlag and Stein, 2007; Sersa et al., 2008; Tsai et al., 2008). Even though sophisticated numerical mathematical models are used to plan effective ECT, these models assume that the chemotherapeutic drug is equally distributed in the tissue of interest and focus on the optimization of the electric field distribution needed to cover the whole tissue area of interest (Miklavcic et al., 2010). To the best of our knowledge, the role of perfusion and metabolism is not included in PEIT and ECT planning procedures today. Due to the amount of emerging applications where drugs are introduced into tissue for local therapy, there is need for a mathematical, mechanistic model that will predict the temporal and spatial distribution of chemical species in living perfused tissues.

The goal of this study, therefore, is to develop an analytical model to predict distribution of chemical species inside tissues in time and space in perfused tissues. Based on a nonhomogeneous mass transport equation we analyzed a 1-D transient and steady-state concentration of chemical species in living, metabolically active tissue. Heterogeneity of the governing equation of the model is due to two parameters, blood perfusion rate and metabolism, represented as an irreversible uptake of a compound by tissue. Here we demonstrate the steady-state and transient analytical solutions in the range of physiologically relevant parameters. We validated our model on data available from PEIT of liver carcinoma and show that the effective volume of the treated tumor is limited by the liver perfusion level.

Materials and Methods

Physical Model

The dimensional physical model of the system is shown in Figure 1. The figure describes a living tissue in a 1-D Cartesian coordinate system. In this one-dimensional model, we approximated the tissue as a cylinder and the source covers the whole cross section. Therefore, there is diffusion in only one direction, outside from the central plane that is a source. Constant concentration is applied at one side of the tissue and is used as a boundary condition in this study. This

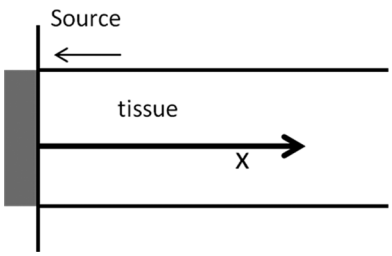

Figure 1. Analyzed physical system scheme.

boundary condition is valid when the quantity of the distributed compound is much less than that in the source, or if a constant rate infusion is performed. This assumption is practical for PEIT, with a multipronged injection with high dosage, or during continuous spinal anesthesia (Denny and Selander, 1998; Kuang et al., 2009). Furthermore, this assumption can be used when the chemicals are produced by devices implanted with living cells, for example, growth factor secretion by encapsulated mesenchymal stromal cells, as appeared in work by Barminko et al. (2011). We assumed that the tissue is significantly long in relation to the source plane; therefore, the system is described as a semi-infinite solid bar. The initial concentration of the introduced compound in the tissue is zero.

Governing Equations

Based on mass conservation laws, the general equation that describes the transport of chemical species inside living tissue is:

$$\frac{\partial C}{\partial t} + v \cdot \nabla C = D\nabla^2 C + R_e(C) + R_m(C) + R_d(C) \tag{1}$$

where C [M] is the concentration of chemical species, t [s] is the time following the compound introduction, v [$\mathrm{cm} \cdot \mathrm{s}^{-1}$] is the fluid velocity, D [$\mathrm{cm}^2 \cdot \mathrm{s}^{-1}$] is Fick's diffusion coefficient of the chemical in the tissue, R_e [$\mathrm{M} \cdot \mathrm{s}^{-1}$] is the rate of chemical elimination by body fluids, R_m [$\mathrm{M} \cdot \mathrm{s}^{-1}$] is the rate of chemical species uptake by the tissue, and R_d [$\mathrm{M} \cdot \mathrm{s}^{-1}$] is the chemical self-degradation rate.

To find the exact solution to Equation (1) the parameters must be measured experimentally; those, however, are not available yet. Therefore, in this work we used the following simplifications. Following Saltzman and Radomsky (1991) we neglected the fluid convection. Based on Smith et al. (1993) and Levitt and Levitt (1998) we assumed that the rate of chemical elimination due to perfusion and absorption by tissue is a linear function of the concentration. In addition, we assumed that R_d is much smaller than its clearance or tissue metabolism rates. Hence, in 1-D with a Cartesian coordinate system Equation (1) transforms to the simplified version as Equation (2):

$$\frac{dC}{dt} = D \cdot \frac{d^2 C}{dx^2} - (w_p + k_b) \cdot C \tag{2}$$

where x [cm] is the distance from the source plane (Figure 1), w_p [s^{-1}] is the tissue perfusion rate, and k_b [s^{-1}] is the first-order absorption rate constant. In this model, the chemical absorption includes the compound uptake by cells and irreversible absorption of the compound by other tissue elements such as extracellular matrix and cell membrane.

Boundary Conditions

The starting concentration of the introduced chemical in the tissue is 0, and a constant concentration is maintained at the source plane (Figure 1). Therefore, the boundary conditions (BC) and the initial conditions (IC) for Equation (2) are as follows:

$$BC : C(0, t) = B \tag{3}$$

$$IC : C(x,0) = 0 \tag{4}$$

where B [M] is the concentration of the chemical at the source plane as described in Figure 1.

Results and Discussion

Parametric Study

Tissues have various geometries and properties; therefore, we introduce a general dimensionless analysis in the following section. We define the following dimensionless variables:

$$W = \frac{w_p[1/s] + k_b[1/s]}{D[m^2/s]} \cdot x^2[m^2] \tag{5}$$

$$F = \frac{D \cdot [m^2/s] \cdot t[s]}{x^2[m^2]} \tag{6}$$

$$\theta = \frac{C[M]}{B[M]} \tag{7}$$

where W is the dimensionless metabolic rate, F is the dimensionless time, and θ is thedimensionless concentration. In addition, we define a new dimensionless coordinate $\sqrt{W}$, in terms of which we will solve the equation.

The dimensionless form of Equation (2) as a function of $(\sqrt{W})$ and (F · W) is.

$$\frac{\partial\theta}{\partial(F \cdot W)} = \frac{\partial^2\theta}{\partial(\sqrt{W})^2} - \theta \tag{8}$$

The dimensionless forms of the BC and IC appear in Equations (9) and (10) respectively:

$$BC : \theta(\sqrt{W} = 0, F \cdot W) = 1 \tag{9}$$

$$IC : \theta(\sqrt{W}, F \cdot W = 0) = 0 \tag{10}$$

Steady-State Concentration Profile

Steady state shows the concentration profile of the chemical compound in living tissue at infinite time after the chemical introduction initiation. The steady-state condition implies $\frac{\partial\theta}{\partial(F \cdot W)} = 0$. Equations (11) and (12) show the solution for concentration profile for the steady-state $(\sqrt{W})$ and $(F \cdot W)$ coordinate system:

$$\frac{\partial^2\theta}{\partial(\sqrt{W})^2} - \theta = 0 \tag{11}$$

$$\theta_{ss}(\sqrt{W}) = \exp(-\sqrt{W}) \tag{12}$$

where θ_{ss} is the concentration at the steady state.

Steady-State Drug Penetration Depth

One of the most important outcomes of our model is the method to calculate the depth at which the introduced chemical compound is at an active concentration; x_t is defined as the depth at which the compound concentration is at the effective level ε, and ε is the dimensionless minimum fraction of the chemical compound that still has the desired functional biological effect. The solution for dimensionless active drug penetration depth X_t is shown as follows:

$$\theta_{ss} = \exp(-\sqrt{W}) = \varepsilon \tag{13}$$

$$\sqrt{W} = \ln\frac{1}{\varepsilon} = X_t \tag{14}$$

The dimensional solution for x_t is

$$x_t = \sqrt{W} \cdot \sqrt{\frac{D}{w_p + k_b}} = \ln\frac{1}{\varepsilon} \cdot \sqrt{\frac{D}{w_p + k_b}} = \ln\frac{1}{\varepsilon} \cdot \delta_b \tag{15}$$

where x_t [cm] is the active chemical compound penetration depth and characteristic length δ_b [cm] is defined as follows:

$$\delta_b = \sqrt{\frac{D[cm^2 s^{-1}]}{w_p[s^{-1}] + k_b[s^{-1}]}} \tag{16}$$

The results for the steady-state active penetration depth and steady-state concentration for parameters described in Table I, which were chosen for the parametric

Table I. Model inputs and values investigated in the parametric study

Variable	Physical property	Unit	Investigated range
t	Time from the compound introduction	s	1×10^{-3}–1×10^{3}
X	Distance from the source	m	1×10^{-3}–1×10^{-1}
B	Boundary concentration	M	1
D	Diffusion coefficient of a chemical compound in the tissue	$m^2 \cdot s^{-1}$	5×10^{-6}
$w_p + k_b$	Total first-order elimination rate constant	s^{-1}	1×10^{-4}–7×10^{-2}
ε	Minimal fraction of the chemical compound that causes a desired effect		4×10^{-1}–9.5×10^{-1}

study, are presented in Figure 2. Figure 2(a) shows the dimensionless active penetration depth for ε of 0.4–0.95 as described in Equation (14). Figure 2(b) shows the dimension penetration depth as a function of ε, w_p, and k_b. Figure 2(c) describes the dimensionless concentration profile for a range of dimensionless metabolic rates (W). Figure 2(d) shows the steady-state concentration profile in living tissue as a function of the distance from the source, perfusion, and absorption rates.

Analysis of Figure 2 reveals certain trends relevant to maximum possible concentration of a chemical compound in living tissue. Figures 2(a) and 2(b) show that large active penetration depth is possible if a small fraction of the chemical compound has the desired effect. The exponential dependence between ε and X_t is particularly important for the application of compounds that have long-term cytotoxic effects in concentrations much smaller than the concentrations needed for the locally desired result. For example, in percutaneous ethanol therapy 98% ethanol is usually directly injected into tumors, and the procedure is effective for 2–3 cm tumor size. However, it was recently shown that much smaller concentrations of ethanol cause a modified gene expression profile and lead to cell apoptosis (Castaneda and Rosin-Steiner, 2006). Therefore, using the proposed model may be useful for the evaluation of the low-concentration-affected areas before treatment. Figures 2(b)–(d) reveal the impact of metabolic activities of the tissue. In this study, we investigated the

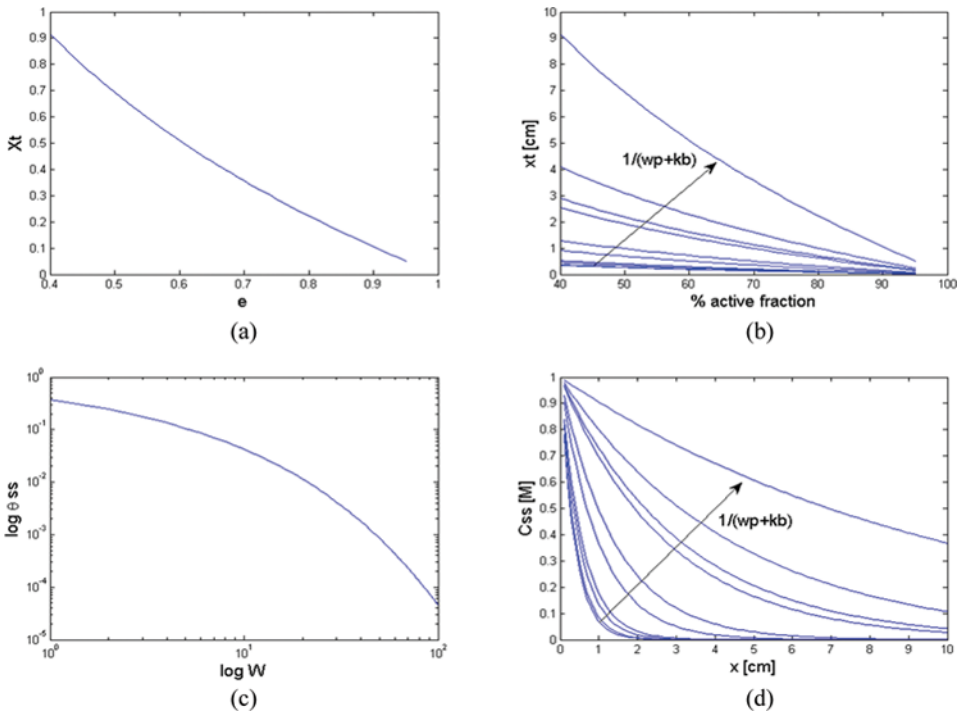

Figure 2. (a) Dimensionless drug penetration depth (X_t) as a function of minimum active concentration (ε), (b) drug penetration depth as a function of a drug fraction in %, (c) dimensionless steady-state concentration as a function of dimensionless metabolic rate (W), and (d) drug steady-state concentration for various perfusion and absorption rates. (Figure provided in color online.)

impact of tissue perfusion rate and irreversible uptake by cells and tissues. Figure 2(c) shows that increased metabolic rate decreases the maximum concentration of the chemical compound in the steady-state at any location. Figures 2(b) and 2(d) demonstrate the dimensional impact of a range of physiologically relevant perfusion/absorption rates on the steady-state concentration and on maximum active penetration depth. Therefore, our findings suggest that chemical dosages can be different for different tissue types and must be correlated with tissue metabolic rates.

Transient Solution

For practical applications, it is valuable to know the temporal and spatial concentration profile following the chemical introduction. To solve inhomogeneous Equation (8) with initial and boundary conditions described in Equations (9) and (10) we use a Duhamel theorem as described in the appendix. The solution described in the appendix leads to the analytical solution of a dimensionless concentration as a function of $(\sqrt{W})$ and $(F \cdot W)$ as follows:

$$\theta(\sqrt{W}, F \cdot W) = \frac{\sqrt{W} \cdot e^{-F \cdot W}}{2\sqrt{\pi}} \int_{\tau=0}^{F \cdot W} \frac{e^{\tau - \frac{W}{4(F \cdot W - \tau)}}}{(F \cdot W - \tau)^{3/2}} d\tau \tag{17}$$

Figure 3 shows the solution for Equation (17). Transient concentration is calculated for various dimensionless metabolic rates. We solved the integral in Equation (17) numerically using MATLAB software (ver. 3.5, Mathworks, Natick, Mass.) with the parameters that appear in Table I. The dimensionless analyses were performed as described in Equations (5)–(7).

Figure 3 describes the dimensionless concentration profile in living tissue as a function of metabolic rate; however, sometimes it is more convenient to analyze transient concentration profiles as a function of time and location. We defined the dimensionless time F in Equation (6), and Equation (18) defines the dimensionless

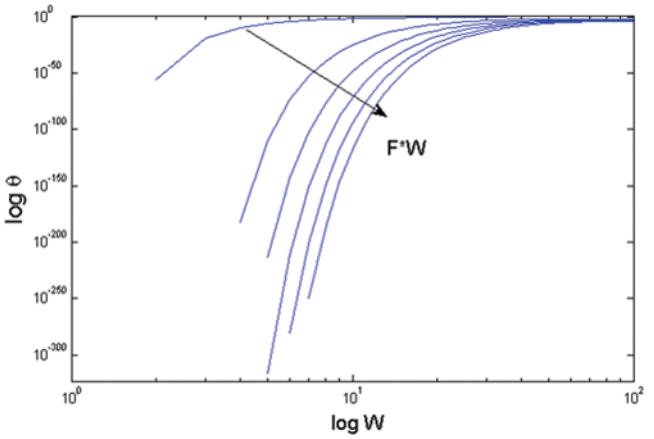

Figure 3. Transient dimensionless concentration as a function of dimensionless perfusion and time. (Figure provided in color online.)

coordinate X:

$$X = \frac{x[cm]}{\delta_b[cm]} \tag{18}$$

Transfer of Equations (2)–(4) to the dimensionless form in the X and F coordinates leads to Equations (19)–(21):

$$\frac{\partial\theta}{\partial F} = \frac{\partial^2\theta}{\partial X^2} - \theta \tag{19}$$

$$BC : \theta(X = 0, F) = 1 \tag{20}$$

$$IC : \theta(X, F = 0) = 0 \tag{21}$$

Following the methodology developed for transient solution (appendix) we solved Equation (19) with the boundary and initial conditions as described in Equations (20) and (21) as follows:

$$\theta(X, F) = \frac{X \cdot e^{-F}}{2\sqrt{\pi}} \int_{\tau=0}^{F} \frac{e^{\tau - \frac{X^2}{4(F-\tau)}}}{(F-\tau)^{3/2}} d\tau \tag{22}$$

The dimensional form of Equation (22) appears in Equation (23):

$$C(x, t) = \frac{xB}{\sqrt{4\pi D}} e^{-(w_p + k_b)t} \int_{\tau=0}^{t} \frac{e^{(w_p+k_b)\tau - \frac{x^2}{4D(t-\tau)}}}{(t-\tau)^{3/2}} d\tau \tag{23}$$

Figure 4 shows the chemical compound concentration profile as a function of time and distance from the source plane for a specific matabolic rate. Figure 4(a)

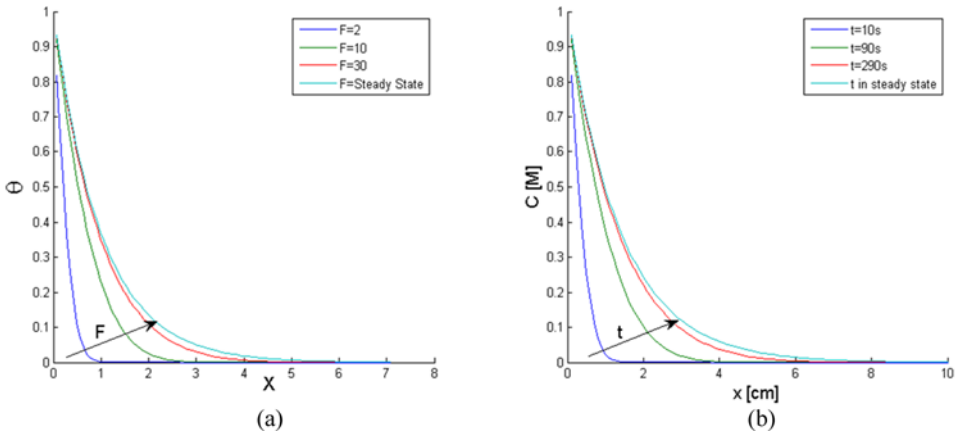

Figure 4. (a) Transient dimensionless concentration as a function of dimensionless time and location for dimensionless perfusion rate $W = 50$, (b) transient concentration as a function of time and location for perfusion rate $w_p + k_b = 5 \times 10^{-3}\,s^{-1}$. (Figure provided in color online.)

describes the dimensionless concentration profile, while Figure 4(b) shows the dimensional concentration profile for data described in Table I.

Figures 3 and 4(a) show the dimensionless profile of the chemical compound concentration as a function of time, location, and metabolic rate.

An interesting additional parameter that describes the system is time to achieve steady state, t_{ss}. To simplify the calculation, we assumed that once the difference between θ and θ_{ss} is less than 10% when steady state is achieved. Using Equation (6) the time to reach steady state is:

$$t_{ss} = F_{ss} \cdot \frac{\delta_b^2}{D} \tag{24}$$

where F_{ss} is a dimensionless time to achieve a steady state, which is found from the solution of Equation (22). Figure 5 shows the dependence of time to steady state on the perfusion rate in dimensionless (Figure 5(a)) and dimensional (Figure 5(b)) forms. Figure 5 reveals a strong dependence of time to steady state on W at low metabolic rates; however, at high metabolic rates time to steady state shows very small dependence on W. This information is valuable since it indicates that the steady state is achieved at different times in different organs. For instance, this finding has an impact on the synchronization of drug injection and application of pulse electric fields during ECT. Specifically, in highly perfused and metabolically active organs, for example, liver, pulses should be applied in proximity to the injection of the chemical agent, before the drug is washed out. However, in tissue with low perfusion and metabolism rate, for example, bone, pulses should be applied for longer periods after drug injection.

Moreover, the injection planning of toxic substances is important because of their effect on non-target tissues and organs. For example, pancreatitis was reported due to ethanol injection in liver (Zardi et al., 2008).

These findings have a broader impact on mass transport analyses in living tissues. For instance, these findings suggest that for effective cell-cell communication the synthesis rate of signaling molecules will be different in organs with different

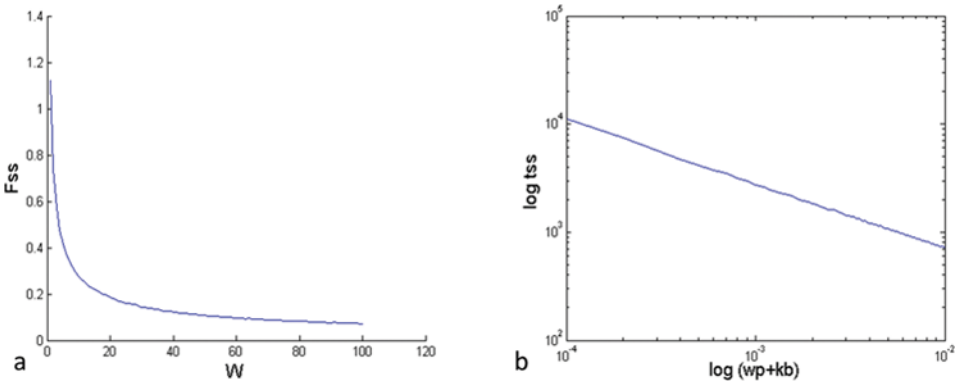

Figure 5. (a) Dimensionless time to steady state as a function of dimensionless metabolic rate, (b) time to reach steady state as function of perfusion and metabolism rates. (Figure provided in color online.)

perfusion and absorption rates. Indeed, cells need to synthesize more signaling molecules in highly perfused organs to deliver a signal for the same distance than in organs with a low perfusion rate.

Practical Example of Local Distribution Model for Percutaneous Ethanol Injection of Liver

To demonstrate the practical application of the developed model we analyzed the clinical application of the direct injection of a chemical compound, PEIT. In this example, we focused on PEIT of a liver.

Although during classic PEIT treatment a 98% ethanol solution is injected into the tumor, recent studies suggest that significantly lower concentrations may be used to induce cell necroses and apoptosis (Castaneda and Rosin-Steiner, 2006; Tapani et al., 1996).

The goal of this part of the study is to demonstrate the possible application of the developed model for liver carcinoma PEIT planning. In this example, we use the data from the low ethanol ablation experiments previously reported in Castaneda and Rosin-Steiner (2006) and Tapani et al. (1996) to analyze the maximum possible ablation area using the methodology developed in the previous sections. For the concentration profile calculation (Equation (23)), we used the parameters given in Table II. Instead of ethanol diffusivity rates in liver, which is unavailable to the best of our knowledge, we used the liver diffusivity for magnetic resonance (MR) contrast agent in liver tumors, as reported by Jia et al. (2008). There the authors measured and built a model for the diffusion coefficient of an extracellular small molecule in a liver tumor (Jia et al., 2008).

For demonstration purposes we assumed that blood and tissue have the same density ($1.059\ \mathrm{gr}\cdot\mathrm{mL}^{-1}$ has been measured for liver (Shephard, 1991) and $1040\text{–}1055\,\mathrm{gr}\cdot\mathrm{mL}^{-1}$ for blood (Kenner, 1989)); therefore, we simplified the perfusion rate as follows:

$$w_p = 45.5\mathrm{mL} \times 100\mathrm{gr}^{-1}\mathrm{min}^{-1} = 7.5 \times 10^{-3}\mathrm{s}^{-1} \tag{25}$$

The transient solution for the ethanol concentration in liver (with $B = 1$ [M] as the boundary condition at the source) is shown at Figure 6. Figure 6 and the solution of Equation (38) suggest that due to the high perfusion of liver the maximum distance from the source where significant concentration of ethanol can be found in the steady state is about 3 cm (a 6-cm diameter of the affected area). Our model

Table II. Diffusion and metabolic parameters for PEIT model

Variable	Physical meaning	Value	Reference
D	Diffusivity	$2.2 \times 10^{-3}\,\mathrm{cm\,s}^{-1}$	Jia et al., 2008
k_b	First-order kinetics of ethanol absorption in liver	$8.1 \times 10^{-4}\,\mathrm{s}^{-1}$	Smith et al., 1993
w_p	Average perfusion rate of small rat liver tumor	$45.5\,\mathrm{mL}\ 100\mathrm{gr}^{-1}\mathrm{min}^{-1}$	Muller and Rogga, 1995

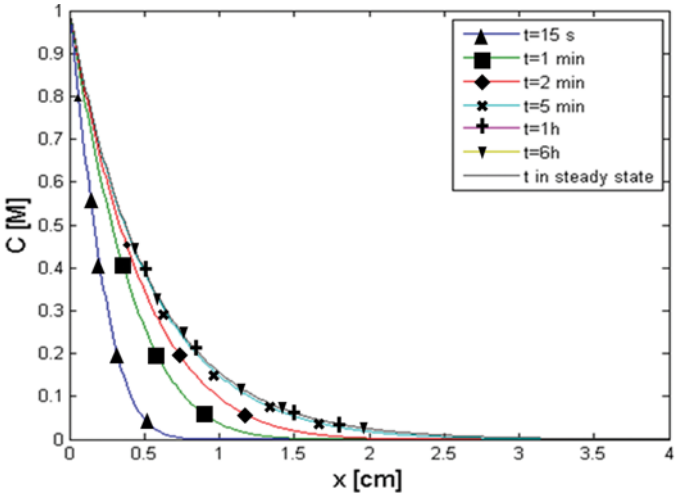

Figure 6. Ethanol concentration in a liver as a function of location and time. (Figure provided in color online.)

prediction correlates with the clinical data, where successful treatments are reported on PEIT of hepatocellular carcinoma in patients with lesions of up to 5 cm in diameter (Figure 7) (Kuang et al., 2009; Livraghi et al., 1995).

Previous works (Castaneda and Rosin-Steiner, 2006; Tapani et al., 1996) reported on the critical time exposures needed to inactivate hepatomelanoma cells

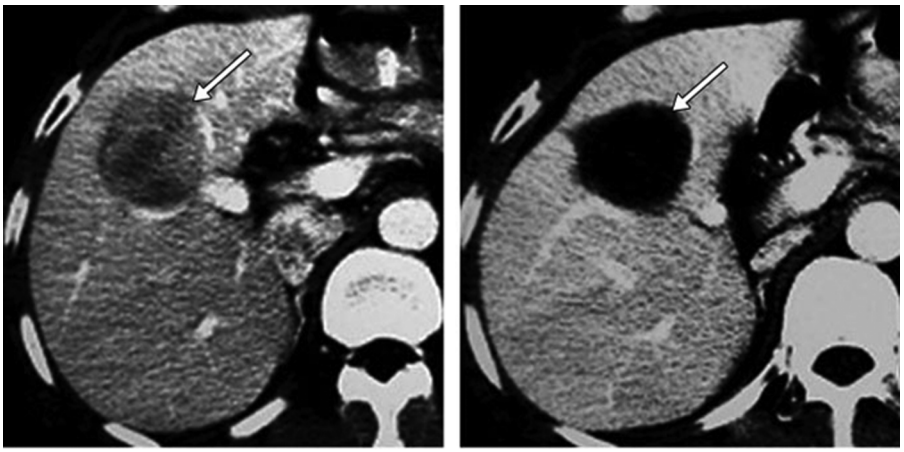

(a) (b)

Figure 7. Transverse contrast-enhanced CT scans in 55-year-old female patient who underwent multipronged ethanol ablation of HCC at unfavorable location. (a) Pre-ablation scan (portal venous phase) shows 4.1×4.5 cm tumor (arrow) located above bifurcation of left and right portal veins; (b) scan obtained 1 month after ethanol ablation (one session, 40 mL of ethanol injected) shows hypoattenuating change of whole target tumor area (arrow). Image adopted from Kuang et al. (2009) with permission.

Table III. Toxic ethanol concentration for various exposure durations

Time [s]	Critical concentration %	ε	Reference	Point N on Fig. 8
15	40	0.4	Tapani et al., 1996	1
300	20	0.2	Tapani et al., 1996	2
600	15	0.15	Tapani et al., 1996	3
3600	10	0.1	Tapani et al., 1996	4
21600	0.046	0.0046	Castaneda and Rosin-Steiner, 2006	5

at specific low concentrations of ethanol. Using Equation (15), the solution to Figure 6, and data from Tables II and III, we calculated the active penetration depth (x_t), the distance from the source plane at which cells will be killed at the concentration and time defined in Table III. Figure 8 shows $x_t$as a function of time.

Figure 7 suggests that given in vitro experiments on chemical substance toxicity effect, our model might predict the effective range of the chemical substance in vivo in metabolically active tissue.

It is important to point out that we present a primary mathematical model with only one set of boundary conditions assumed. Multiple situations will demand solution with different boundary conditions appropriate to the specific condition. Furthermore, experimental data are still needed for the model's in vivo validation. Our analyses, however, add complexity, based on physiological factors, to previously reported models on chemical distribution in living tissues. We emphasize the need to include important properties of living tissues, such as perfusion and metabolism, to mass transport modeling in tissues.

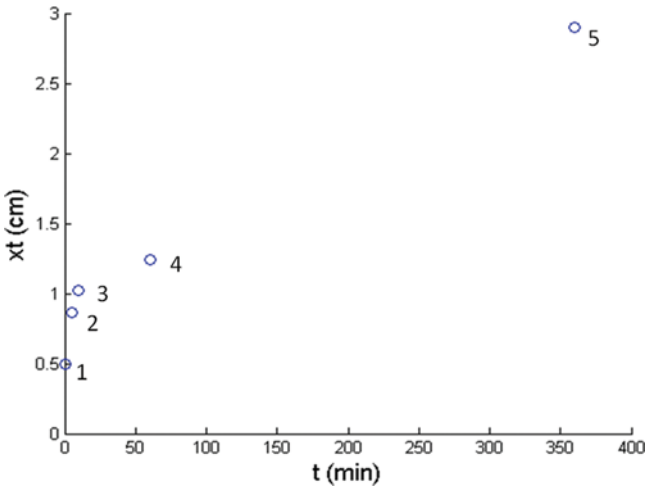

Figure 8. Distance from the injection point at which ethanol causes liver tumor ablation by necrosis (points 1–4) and apoptosis (point 5). (Figure provided in color online.)

Conclusions

We report on an analytical model for analysis of temporal and spatial distribution of chemicals in living tissues with first-order-kinetic rate metabolism. Our model suggests that the maximum active distance of an introduced chemical is limited by the tissue perfusion and metabolism rates. Our findings emphasize the need for mathematical planning for therapies that involve local injection of chemical compounds. The benefit of using mathematical models in this case will be significant reduction in preliminary experiments and assessment of long-term toxicity effects at low concentrations. The broader significance of the model developed in this study is that it may contribute to the understanding of in vivo intercellular signaling and morphogenetic gradient propagation.

Acknowledgments

The author acknowledges Prof. Boris Rubinsky from the Department of Mechanical Engineering at the University of California, Berkeley for providing valuable insights on transport phenomena behavior in living tissues.

References

Andre, F., and Mir, L. M. (2004). DNA electrotransfer: Its principles and an updated review of its therapeutic applications, *Gene Ther.*, **11**, S33–S42.

Baish, J. W., Stylianopoulos, T., Lanning, R. M., Kamoun, W. S., Fukumura, D., Munn, L. L., and Jain, R. K. (2011). Scaling rules for diffusive drug delivery in tumor and normal tissues, *Proc. Natl. Acad. Sci. U.S.A.*, **108**, 1799–1803.

Barminko, J., Kim, J. H., Otsuka, S., Gray, A., Schloss, R., Grumet, M., and Yarmush, M. L. (2011). Encapsulated mesenchymal stromal cells for in vivo transplantation, *Biotechnol. Bioeng.*, **108**, 2747–2758.

Bennedbaek, F. N., Karstrup, S., and Hegedus, L. (1997). Percutaneous ethanol injection therapy in the treatment of thyroid and parathyroid diseases, *Eur. J. Endocrinol.*, **136**, 240–250.

Castaneda, F., and Rosin-Steiner, S. (2006). Low concentration of ethanol induce apoptosis in HepG2 cells: Role of various signal transduction pathways, *Int. J. Med. Sci.*, **3**, 160–167.

Cemazar, M., Milacic, R., Miklavcic, D., Dolzan, V., and Sersa, G. (1998). Intratumoral cisplatin administration in electrochemotherapy: Antitumor effectiveness, sequence dependence and platinum content, *Anti-Cancer Drugs*, **9**, 525–530.

Denny, N. M., and Selander, D. E. (1998). Continuous spinal anesthesia, *Br. J. Anaesth.*, **81**, 590–597.

DiMaio, C. J., DeWitt, J. M., and Brugge, W. R. (2011). Ablation of pancreatic cystic lesions: The use of multiple endoscopic ultrasound-guided ethanol lavage sessions, *Pancreas*, **40**, 664–668.

Doherty, M. M., Hughes, P. J., Korszniak, N. V., and Charman, W. N. (1995). Prolongation of lidocaine-induced epidural anesthesia by medium molecular weight hyaluronic acid formulations: Pharmacodynamic and pharmacokinetic studies in the rabbit, *Anesth. Analg.*, **80**, 740–746.

Eungdamrong, N. J., and Iyengar, R. (2004). Modeling cell signaling networks, *Biol. Cell*, **96**, 355–362.

Gangi, A., Kastler, B., Klinkert, A., and Dietemann, J. L. (1994). Injection of alcohol into bone metastases under CT guidance, *J. Comput. Assist. Tomogr.*, **18**, 932–935.

Glass, L. F., Jaroszeski, M., Gilbert, R., Reintgen, D. S., and Heller, R. (1997). Intralesional bleomycin-mediated electrochemotherapy in 20 patients with basal cell carcinoma, *J. Am. Acad. Dermatol.*, **37**, 596–599.

Gothelf, A., Mir, L. M., and Gehl, J. (2003). Electrochemotherapy: Results of cancer treatment using enhanced delivery of bleomycin by electroporation, *Cancer Treat. Rev.*, **29**, 371–387.

Goya, N., Ishikawa, N., Ito, F., Ryoji, O., Tokumoto, T., Toma, H., and Yamaguchi, Y. (1999). Ethanol injection therapy of the prostate for benign prostatic hyperplasia: Preliminary report on application of a new technique, *J. Urol.*, **162**, 383–386.

Heilo, A., Sigstad, E., Fagerlid, K. H., Haskjold, O. I., Groholt, K. K., Berner, A., Bjoro, T., and Jogensen, L. H. (2011). Efficacy of ultrasound-guided percutaneous ethanol injection treatment in patients with a limited number of metastatic cervical lymph nodes from papillary thyroid carcinoma, *J. Clin. Endocrinol. Metab.*, **96**, 2750–2755.

Heller, R., Gilbert, R., and Jaroszeski, M. J. (1999). Clinical applications of electrochemotherapy, *Adv. Drug Deliv. Rev.*, **35**, 119–129.

Jia, G., O'Dell, C., Heverhagen, J. T., Yang, X., Liang, J., Jacko, R. V., Sammet, S., Pellas, T., Cole, P., and Knopp, M. V. (2008). Colorectal liver metastases: Contrast agent diffusion coefficient for quantification of contrast enhancement heterogeneity at MR imaging, *Radiology*, **248**, 901–909.

Kenner, T. (1989). The measurement of blood density and its meaning, *Basic Res. Cardiol.*, **84**, 111–124.

Kim, Y. J., Raman, S. S., Yu, N. C., and Lu, D. S. K. (2005). MR-guided percutaneous ethanol injection for hepatocellular carcinoma in a 0.2 T open MR system, *J. Magn. Reson. Imaging*, **22**, 566–571.

Kuang, M., Lu, M.-D., Xie, X.-Y., Xu, H.-X., Xu, Z.-F., Liu, G.-J., Yin, X.-Y., Huang, J.-F., and Lencioni, R. (2009). Ethanol ablation of hepatocellular carcinoma up to 5.0 cm by using a multipronged injection needle with high-dose strategy, *Radiology*, **253**, 552–561.

Kwon, Y. (2001). *Handbook of Essential Pharmacokinetics, Pharmacodynamics and Drug Metabolism for Industrial Scientists*, Springer, New York.

Lee, S. J., and Ahn, I.-M. (2005). Effectiveness of percutaneous ethanol injection therapy in benign nodular and cystic thyroid diseases: Long-term follow-up experience, *Endocr. J.*, **52**, 455–462.

Levitt, M. D., and Levitt, D. G. (1998). Use of a two-compartment model to assess the pharmacokinetics of human ethanol metabolism, *Alcoholism*, **22**, 1680–1688.

Livraghi, T., Giorgio, A., Marin, G., Salmi, A., de Sio, I., Bolondi, L., Pompili, M., Brunello, F., Lazzaroni, S., and Torzilli, G. (1995). Hepatocellular carcinoma and cirrhosis in 746 patients: Long-term results of percutaneous ethanol injection, *Radiology*, **197**, 101–108.

Miklavcic, D., Snoj, M., Zupanic, A., Kos, B., Cemazar, M., Kropivnik, M., Bracko, M., Pecnik, E., Gadzijev, E., and Sersa, G. (2010). Towards treatment planning and treatment of deep-seated solid tumors by electrochemotherapy, *Biomed. Eng. Online*, **9**. doi: 10.1186/1475-925X-9-10.

Mir, L. M., Orlowski, S. P., Belehradek, Jr., J., and Paoletti, C. (1991). Electrochemotherapy potentiation of antitumour effect of bleomycin by local electric pulses, *Eur. J. Cancer Clin. Oncol.*, **27**, 68–72.

Mir, L. M., Gehl, J., Sersa, G., Collins, C. G., Garbay, J.-R., Billard, V., Geertsen, P. F., Rudolf, Z., O'Sullivan, G. C., and Marty, M. (2006). Standard operating procedures of the electrochemotherapy: Instructions for the use of bleomycin or cisplatin administered either systemically or locally and electric pulses delivered by the Cliniporator^{TM} by means of invasive or non-invasive electrodes, *Eur. J. Cancer Suppl.*, **4**, 14–25.

Muller, G., and Rogga, A. (1995). *Laser-Induced Interstitial Thermotheraphy*, SPIE–The International Society for Optical Engineering, Bellingham, WA.

Myers, M. R. (1996). A numerical investigation into factors affecting anesthetic distribution during spinal anesthesia, *J. Biomech.*, **29**, 139–149.

Nakayama, J., Kokuba, H., Kobayashi, J., Yoshida, Y., and Hori, Y. (1997). Experimental approaches for the treatment of murine B16 melanomas of various sizes. I: Local

injection of ethanol with a combination of interleukin-2 or microwaval hyperthermia for B16 melanomas with a size of less than 7 mm in diameter, *J. Dermatol. Sci.*, **15**, 75–81.

Nakayama, A., Kuwahara, F., and Liu, W. 2011. A general set of bioheat transfer equations based on volume averaging theory, in *Porous Media: Applications in Biological Systems and Biotechnology*, ed. K. Vafai, CRC Press, Boca Raton, Fla.

Özisik, M. N. (1993). *Heat Conduction, 2nd ed.*, John Wiley & Sons, New York.

Paganin-Gioanni, A., Bellard, E., Escoffre, J. M., Rols, M. P., Teissié, J., and Golzio, M. (2011). Direct visualization at the single-cell level of siRNA electrotransfer into cancer cells, *Proc. Natl. Acad. Sci. U.S.A.*, **108**, 10443–10447.

Papini, E., Panunzi, C., Pacella, C. M., Bizzarri, G., Fabbrini, R., Petrucci, L., Pisicchio, G., and Nardi, F. (1993). Percutaneous ultrasound-guided ethanol injection: A new treatment of toxic autonomously functioning thyroid nodules? *J. Clin. Endocrinol. Metab.*, **76**, 411–416.

Pennes, H. H. (1948). Analysis of tissue and arterial blood temperatures in the resting human forearm, *J. Appl. Physiol.*, **1**, 93–122.

Ross, B. K., Coda, B., and Heath, C. H. (1992). Local anesthetic distribution in a spinal model: A possible mechanism of neurologic injury after continuous spinal anesthesia, *Reg. Anesth.*, **17**, 69–77.

Saltzman, W. M. (2001). *Drug Delivery: Engineering Principles for Drug Therapy*, Oxford University Press, New York.

Saltzman, W. M., and Radomsky, M. L. (1991). Drugs released from polymers: Diffusion and elimination in brain tissue, *Chem. Eng. Sci.*, **46**, 2429–2444.

Schlag, P. M., and Stein, U. (2007). *Regional Cancer Therapy*, Humana Press, Danvers, Mass.

Sersa, G., Miklavcic, D., Cemazar, M., Rudolf, Z., Pucihar, G., and Snoj, M. (2008). Electrochemotherapy in treatment of tumours, *Eur. J. Surg. Oncol.*, **34**, 232–240.

Shen, H., Hu, Y., and Saltzman, W. M. (2006). DNA diffusion in mucus: Effect of size, topology of DNAs, and transfection reagents, *Biophys. J.*, **91**, 639–644.

Shephard, R. J. (1991). *Body Composition in Biological Anthropology*, Cambridge University Press, New York.

Shitzer, A. (2011). Cryosurgery: Analysis and experimentation of cryoprobes in phase changing media, *J. Heat Transfer*, **133**, 011005.

Smith, G. D., Shaw, L. J., Maini, P. K., Ward, R. J., Peters, T. J., and Murray, J. D. (1993). Mathematical modelling of ethanol metabolism in normal subjects and chronic alcohol misusers, *Alcohol Alcohol.*, **28**, 25–32.

Tapani, E., Taavitsainen, M., Lindros, K., Vehmas, T., and Lehtonen, E. (1996). Toxicity of ethanol in low concentrations, *Acta Radiol.*, **37**, 923–926.

Tsai, W. L., Cheng, J. S., Lai, K. H., Lin, C. P., Lo, G. H., Hsu, P. I., Yu, H. C., Lin, C. K., Chan, H. H., Chen, W. C., Chen, T. A., Li, W. L., and Liang, H. L. (2008). Clinical trial: Percutaneous acetic acid injection vs. percutaneous ethanol injection for small hepatocellular carcinoma—A long-term follow-up study, *Aliment. Pharmacol. Ther.*, **28**, 304–311.

Ummenhofer, W. C., Arends, R. H., Shen, D. D., and Bernards, C. M. (2000). Comparative spinal distribution and clearance kinetics of intrathecally administered morphine, Fentanyl, Alfentanil, and Sufentanil, *Anesthesiology*, **92**, 739–753.

Upton, R., Runciman, W. B., and Mather, L. E. (1991). Regional pharmacokinetics III. Modeling methods, *Biopharm. Drug Dispos.*, **12**, 1–15.

Zardi, E., Di Matteo, F., Santini, D., Uwechie, V., Crucitti, P., Carassiti, M., Picardi, A., Perrella, E., Caricato, M., Tonini, G., Coppola, R., and Afeltra, A. (2008). Pancreatitis after percutaneous ethanol injection into HCC: A minireview of the literature, *J. Exp. Clin. Cancer Res.*, **27**, 28. doi: 10.1186/1756-9966-1127-1128.

Appendix: Solution of Heterogeneous Heat Transfer Equation Using the Duhamel Theorem

The problem for mass transfer in perfused tissue is described in Equation (1A) with boundary and initial conditions that appear in Equations (2A) and (3A):

$$\frac{\partial\theta}{\partial F} = \frac{\partial^2\theta}{\partial \mathrm{X}^2} - \theta \tag{1A}$$

$$BC : \theta(X = 0, F) = 1 \tag{2A}$$

$$IC : \theta(X, F = 0) = 0 \tag{3A}$$

To solve Equation (1A) we make the following substitution:

$$\theta = g \cdot \exp(-F \cdot W) \tag{4A}$$

Substituting Equation (4A) into Equation (1A), we develop Equation (5A) as follows:

$$\frac{\partial g}{\partial(F \cdot W)} = \frac{\partial^2 g}{\partial(\sqrt{W})^2} \tag{5A}$$

Substitution of Equation (4A) into the boundary and initial conditions (Equations (2A) and (3A)) leads to the following transformed boundary and initial conditions:

$$BC : g(0, F \cdot W) = \exp(F \cdot W) = f(\tau) \tag{6A}$$

$$IC : g(\sqrt{W}, F \cdot W = 0) = 0 \tag{7A}$$

Equation (5A) with the boundary and initial conditions described in Equations (6A) and (7A) is a homogeneous heat equation with time-dependent boundary conditions. To solve Equation (5A) with the initial and boundary conditions described, we use the Duhamel theorem and base our solution on Özisik (1993). Using the Duhamel theorem we first solve the following auxiliary problem:

$$\frac{\partial\Phi}{\partial(F \cdot W)} = \frac{\partial^2\Phi}{\partial(\sqrt{W})^2} \tag{8A}$$

$$BC : \Phi(0, F \cdot W) = 1 \tag{9A}$$

$$IC : \Phi(\sqrt{W}, F \cdot W = 0) = 0 \tag{10A}$$

The solution of the auxiliary problem Φ and g are related through the Duhamel theorem as:

$$g(\sqrt{W}, F \cdot W) = \int_{\tau=0}^{F \cdot W} f(\tau) \frac{\partial \Phi(\sqrt{W}, F \cdot W - \tau)}{\partial(\sqrt{W})} d\tau \tag{11A}$$

The solution of the auxiliary problem is:

$$\Phi(\sqrt{W}, F \cdot W) = ercf\left(\frac{\sqrt{W}}{\sqrt{4F \cdot W}}\right) \tag{12A}$$

Therefore:

$$\frac{\partial \Phi(\sqrt{W}, F \cdot W - \tau)}{\partial(\sqrt{W})} = \frac{\sqrt{W}}{\sqrt{4\pi(F \cdot W - \tau)^{3/2}}} e^{-\frac{W}{4(F \cdot W - \tau)}} \tag{13A}$$

and:

$$g(\sqrt{W}, F \cdot W) = \frac{\sqrt{W}}{\sqrt{4\pi}} \int_{\tau=0}^{F \cdot W} \frac{f(\tau)}{(F \cdot W - \tau)^{3/2}} e^{-\frac{W}{4(F \cdot W - \tau)}} d\tau = \frac{\sqrt{W}}{\sqrt{4\pi}} \int_{\tau=0}^{F \cdot W} \frac{e^{\tau}}{(F \cdot W - \tau)^{3/2}} e^{-\frac{W}{4(F \cdot W - \tau)}} d\tau \tag{14A}$$

Therefore, the transient solution for the dimensionless concentration in the perfused tissue is

$$\theta(\sqrt{W}, F \cdot W) = \frac{\sqrt{W} \cdot e^{-F \cdot W}}{2\sqrt{\pi}} \int_{\tau=0}^{F \cdot W} \frac{e^{\tau - \frac{W}{4(F \cdot W - \tau)}}}{(F \cdot W - \tau)^{3/2}} d\tau \tag{15A}$$